THE JOURNAL OF PHYSICAL CHEMISTRY A

Article

pubs.acs.org/JPCA

Anisotropy and Size Effects on the Optical Spectra of Polycyclic Aromatic Hydrocarbons

Caterina Cocchi,*[,†,‡,∥] Deborah Prezzi,[†] Alice Ruini,[†,‡] Marilia J. Caldas,[§] and Elisa Molinari[†,‡]

[†]Centro S3, CNR-Istituto Nanoscienze, I-41125 Modena, Italy

[‡]Dipartimento di Scienze Fisiche, Informatiche e Matematiche, Università di Modena e Reggio Emilia, I-41125 Modena, Italy

[§]Instituto de Física, Universidade de São Paulo, 05508-900 São Paulo, SP, Brazil

ABSTRACT: The electronic and optical properties of polycyclic aromatic hydrocarbons (PAHs) present a strong dependence on their size and geometry. We tackle this issue by analyzing the spectral features of two prototypical classes of PAHs, belonging to D_{6h} and D_{2h} symmetry point groups and related to coronene as multifunctional seed. While the size variation induces an overall red shift of the spectra and a redistribution of the oscillator strength between the main peaks, a lower molecular symmetry is responsible for the appearance of new optical features. Along with broken molecular orbital degeneracies, optical peaks split and dark states are activated in the low-energy part of the spectrum. Supported by a systematic analysis of the composition and the character of the optical transitions, our results contribute in shedding light to the mechanisms responsible for spectral modifications in the visible and near UV absorption bands of medium-size PAHs.

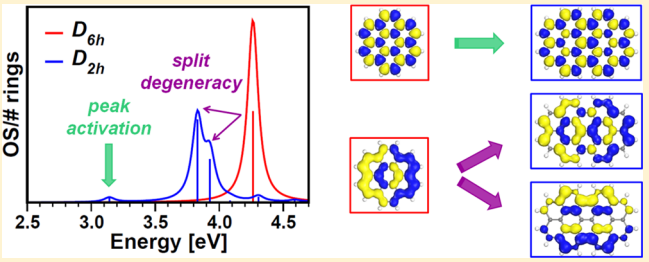

Polycyclic aromatic hydrocarbons (PAHs) are the focus of research in significantly diverse fields, ranging from biochemistry[1] to theoretical chemistry,[2] from molecular electronics[3] to astrochemistry,[4] where PAHs are assigned an important role[5,6] due to their chemical composition and spectral features.[7−11] In this framework, a theoretical identification of the absorption and emission features of these molecules assumes a significant relevance[12,13] since they might drastically vary both upon small structural modifications[14,15] and as a consequence of ionization[16−19] or dehydrogenation.[20−23] In the field of molecular electronics, the interest in medium- and large-sized PAHs is intrinsically connected to graphene, as they are viewed as highly stable graphene molecules.[24] Their intriguing and versatile optical properties,[25,26] combined with their facile bottom-up synthesis[27] and their capability to assemble into $\pi-\pi$ stacked superstructures,[28,29] make them excellent candidates for optoelectronic applications,[3,30] where slight structural variations can trigger different properties and functionalities.[31]

In this article we investigate the effects of size and anisotropy on the optical spectra of PAHs, with the aim of providing a useful reference for understanding and predicting their optical response. To tackle this issue, we focus on two prototypical classes of molecules with D_{6h} and D_{2h} point group symmetry, which are related to coronene, viewed as a multifunctional seed. Indeed, with its high symmetry and specific electronic structure, coronene is one of the most representative medium-sized PAHs.[24] By means of a well-established quantum chemistry approach, we perform a theoretical analysis to identify the size- and anisotropy-induced modifications to the spectral features in the visible and near-UV bands of PAHs. The present study aims at showing that the main effect of size increase, moving from coronene to larger hexagonal PAHs of fixed symmetry, is an oscillator strength variation of the main excitations and a red shift of the whole spectrum, which brings the strong absorption peaks from the UV to the visible energy region, maintaining overall the character of the excitons. Moreover, the additional features produced in the spectra by the anisotropical elongation of coronene in one direction will be investigated; specific focus will be devoted to the effects of symmetry breaking. Finally, it will be clarified that bright excitations in the visible region appear already for the smaller anisotropic molecules, with low mass compared to highly symmetric PAHs.

COMPUTATIONAL METHODS

The results presented in this article are obtained within the framework of Hartree−Fock-based semiempirical methods.[32] This methodology is well tested and reliable to compute the electronic and optical properties of C-conjugated low-dimensional systems,[33−36] including PAHs themselves.[17,37] The AM1 model[38] is adopted for structural optimization [0.4 kcal/(mol·Å) threshold for the forces], whereas the ZINDO/S model,[39] based on configuration interaction (CI) including single excitations only, is employed for the optical spectra.

Special Issue: Franco Gianturco Festschrift

Received: March 27, 2014
Revised: July 1, 2014
Published: July 1, 2014

   dx.doi.org/10.1021/jp503054j | J. Phys. Chem. A 2014, 118, 6507−6513

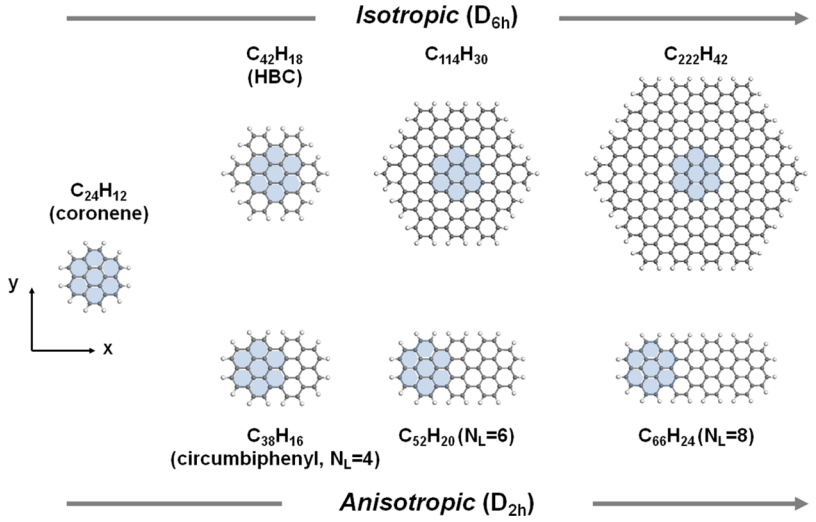

Figure 1. Polycyclic aromatic hydrocarbons (PAHs) investigated in this work. Starting from a coronene molecule as multifunctional seed, we consider both its isotropic and anisotropic size increase. In the first case (above) we obtain hexagonal PAHs with D_{6h} point group symmetry, while in the latter case (below) the hexagonal symmetry is broken and elongated PAHs with D_{2h} point group symmetry are formed.

To better characterize the optical excitations, we introduce the transition density,[40,41] which is defined as

$$\rho^{I}(\mathbf{r}) = \sum_{\alpha,\beta} c^{I}_{\alpha\beta}\phi^{*}_{\beta}(\mathbf{r})\phi_{\alpha}(\mathbf{r}) \tag{1}$$

where ϕ_α (ϕ_β) indicates the occupied (unoccupied) molecular orbitals (MOs) and $c^{I}_{\alpha\beta}$ are the CI coefficients of the Ith excited-state configuration.[42] The transition density is directly related to the transition dipole moment of the Ith excitation:[43]

$$\mu^{I}_{0p} = \langle\Phi_0|\hat{\mathbf{p}}|\Phi_p\rangle = -e\int d^3r\,\hat{\mathbf{r}}\rho^{I}(\mathbf{r}) \tag{2}$$

where $\hat{\mathbf{p}} = -e\hat{\mathbf{r}}$ is the momentum operator, Φ_0 is the ground state Hartree−Fock wave function, and Φ_p is the singly excited configuration, including all the possible Slater determinants obtained by coupling $\phi_\alpha \rightarrow \phi_\beta$ transitions in the given energy window. From eq 2 it is thus clear that the transition density provides a representation of the polarization of the excitation, which can be visualized through a three-dimensional isosurface representation.[44,45] Finally, as the oscillator strength is proportional to the square modulus of the transition dipole moment, the transition density also carries information about the excitation intensity.

Starting from coronene ($C_{24}H_{12}$) as a multifunctional seed, the effects of size and symmetry modifications on the optical properties are investigated by comparing two families of PAHs, characterized by D_{6h} and D_{2h} point group symmetry (see Figure 1). The first class of hexagonal molecules is a Kekulé series of fully benzenoid PAHs with purely armchair edges,[46] obtained by progressively incrementing the number of aromatic rings at the periphery. As a result, the molecules belonging to this group are characterized by an increasing number of armchair-shaped rings per edge, ranging from 2 in hexa-benzo-coronene (HBC, $C_{42}H_{18}$) up to 4 in $C_{222}H_{42}$ (see Figure 1). The second class of molecules is built by anisotropically elongating coronene in one direction only (x axis), as indicated in Figure 1. This gives rise to ribbon-like graphene nanoflakes (GNFs) with armchair-shaped edges. These structures belong to the D_{2h} point group and can be identified through their length (N_L) and width parameters (N_W).[47] The latter is defined as for periodic armchair graphene nanoribbons as the number of C-dimers along the y axis of the molecule (see Figure 1),[48] while N_L is identified as the number of zigzag chains in the x direction, excluding the ends. The coronene-derived GNFs considered here have fixed width of about 7.4 Å (N_W = 7) and increasing length, ranging from about 11 Å (N_L = 4, circumbiphenyl) to almost 20 Å (N_L = 8). Note that in both cases we focus on fully armchair-edged molecules to avoid any spurious open-shell effects, typically associated with the presence of zigzag edges.[49]

RESULTS AND DISCUSSION

The optical absorption spectrum of coronene (Figure 2, top panel) is characterized by an intense peak in the near-UV

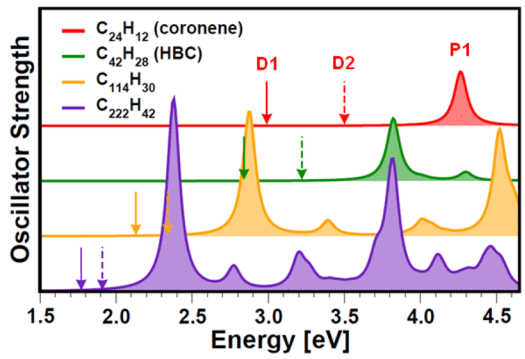

Figure 2. Calculated optical absorption spectra of hexagonal PAHs (D_{6h} point group symmetry) of different sizes. The first intense peak P1 (Clar's β band) is given by doubly degenerate excitations. The lowest energy dipole-forbidden excitations (D1 and D2, α and p bands, according to Clar's notation; see also Table 1) are indicated in the spectra by solid and dashed arrows, respectively. The spectra are obtained by using a Lorentzian broadening of 100 meV.

region (P1, at 4.26 eV, see Table 1) and by two low energy dark excitations in the visible band (D1 and D2 at about 3 and 3.5 eV, respectively). The lowest energy excited states of hexagonal PAHs, corresponding to transitions between the doubly degenerate frontier orbitals (see Figure 4a) and here labeled as D1, D2, and P1, are commonly identified as α, para (p), and β bands, respectively, according to Clar's notation (see e.g. ref

dx.doi.org/10.1021/jp503054j | J. Phys. Chem. A 2014, 118, 6507−6513

Table 1. Summary of the Optical Excitations, I, of Hexagonal PAHs (D_{6h} Point Group Symmetry) Indicated in the Spectra of Figure 2, Including Energy, Oscillator Strength (OS), and Composition in Terms of Molecular Orbital Transitions with the Corresponding CI Coefficients and Weight; Only Contributions Larger than 5% Have Been Included

molecule	I	MO transitions (weight)	$c^{I}_{\alpha\beta}$	energy (eV)	OS
$C_{24}H_{12}$	D1	H → L + 1 (0.47)	−0.683	2.99	0.00
		H − 1 → L (0.47)	0.683		
	D2	H → L (0.49)	−0.700	3.50	0.00
		H − 1 → L + 1 (0.49)	−0.700		
	P1	H → L (0.48)	0.690	4.26	1.96
		H − 1 → L + 1 (0.48)	−0.690		
		H → L + 1 (0.48)	0.690		
		H − 1 → L (0.48)	0.690		
$C_{42}H_{28}$	D1	H → L + 1 (0.44)	−0.665	2.84	0.00
		H − 1 → L (0.44)	0.665		
	D2	H → L (0.47)	−0.684	3.22	0.00
		H − 1 → L + 1 (0.47)	−0.684		
	P1	H → L (0.18)	0.428	3.82	2.25
		H → L + 1 (0.26)	−0.514		
		H − 1 → L (0.26)	−0.514		
		H − 1 → L + 1 (0.18)	−0.428		
		H → L + 1 (0.26)	−0.514		
		H → L (0.18)	−0.428		
		H − 1 → L (0.18)	−0.428		
		H − 1 → L + 1 (0.26)	0.514		
$C_{114}H_{30}$	D1	H → L + 1(0.42)	0.649	2.13	0.00
		H − 1→ L (0.42)	−0.649		
	D2	H → L (0.44)	0.666	2.34	0.00
		H − 1 → L + 1 (0.44)	0.666		
	P1	H → L (0.41)	0.638	2.88	4.53
		H → L + 1 (0.05)	0.228		
		H − 1 → L (0.05)	0.228		
		H − 1 → L + 1 (0.41)	−0.638		
		H → L + 1 (0.41)	−0.638		
		H → L (0.05)	0.228		
		H − 1 → L (0.41)	−0.638		
		H − 1 → L + 1 (0.05)	−0.228		
$C_{222}H_{42}$	D1	H → L + 1 (0.40)	0.629	1.77	0.00
		H − 1 → L (0.40)	−0.629		
	D2	H → L (0.42)	0.646	1.91	0.00
		H − 1 → L + 1 (0.42)	0.646		
	P1	H → L (0.40)	0.635	2.38	6.65
		H − 1 → L + 1 (0.40)	−0.635		
		H → L + 1 (0.40)	0.635		
		H − 1 → L (0.40)	0.635		

15 and references therein). These excitations correspond to symmetry forbidden B_{1u} and B_{2u} states (D1 and D2 in Figure 2) and to a higher energy E_{1u} state, characterized by a twofold degeneracy and by a large oscillator strength (P1 peak). Within the CI approach, we find that P1 stems from the combined transitions of doubly degenerate frontier orbitals (highest occupied MO, HOMO, and lowest unoccupied MO, LUMO; see Table 1). Also D1 and D2 arise from frontier orbital transitions that combine here with opposite sign, hence giving rise to dipole-forbidden transitions. Two additional excitations, one of them doubly degenerate, appear in the spectrum between D2 and P1: they are symmetry-forbidden and come from combinations of transitions between the four occupied and unoccupied MOs closest to the gap.

The features of D1, D2, and P1 can be clearly captured from the transition density plots in Figure 3. The modulation of the positive and negative domains in D1 and D2 provides evidence of the zero dipole moment associated with them, while P1 is characterized by a remarkable polarity. These results are in agreement with the available experimental data[15,50] within about 150 meV, as well as with other predictions obtained within different theoretical approaches.[14,17,51,53] The lowest energy peak is typically identified in experiments as the strongest absorption peak in the UV/vis region. Moreover, as a matter of fact, the lowest dipole-forbidden excitations are also detected in experiments[52] as associated with vibrational modes[17,53] or, in general, with structural deviations from the ideal symmetry, generally adopted in theoretical simulations.[54]

For this series of hexagonal PAHs, Figure 2, from the top to the bottom, indicates that the full optical spectrum, including dark excitations, is red-shifted with increasing size, as expected from the higher delocalization of the relevant molecular orbitals,[55] as recently reported for other PAH series.[15] Specifically, P1 is brought from the UV to the visible range

dx.doi.org/10.1021/jp503054j | J. Phys. Chem. A 2014, 118, 6507−6513

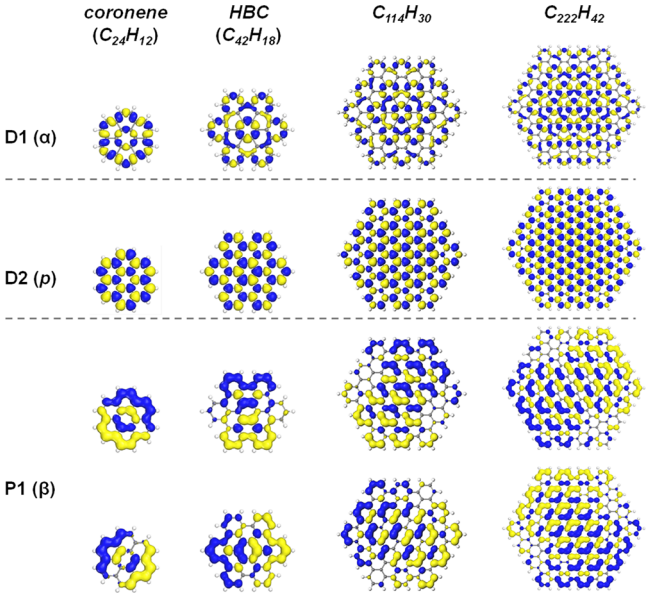

Figure 3. Transition density isosurfaces, computed as in eq 1, of the examined optical excitations of hexagonal PAHs (D_{6h} point group symmetry).

(green), while the lowest-energy dark excitations move from the visible (violet) to the infrared band. As such, P1 undergoes a larger red shift than D1 and D2, in comparison with the spectrum of coronene. The lowest energy excitation of HBC (D1), corresponding to the Clar's α band, is found in our study at 2.84 eV (Table 1). This value is in excellent agreement with recent experimental results of HBC in gas phase[56] and in rare gas matrix:[57] these studies assign the lowest energy excitation of HBC, at 2.86 and 2.85 eV, respectively. In ref 57, also the position of the p band (D2, 3.22 eV, see Table 1) is reported at 3.30−3.35 eV, depending on the embedding gas matrix. Also for this excitation our results compare very well with the experiment within an error of 3%. The first active peak of HBC (P1) stems from our calculations at 3.82 eV (Table 1), also in very good agreement with the experimental data at about 3.7 eV (error of 5%).[57]

As a consequence of the preserved symmetry, the main optical features in all the examined hexagonal PAHs remain unchanged throughout the series (see Figure 2 and Table 1). This is further confirmed by the resulting transition densities shown in Figure 3. In fact, the MOs contributing to the excitations are the same in all the structures, as their character is maintained by the molecular symmetry. In the low energy spectral region, between D2 and P1, only one doubly degenerate excitation appears in the spectra of the larger molecules of this set (HBC, $C_{114}H_{30}$, and $C_{222}H_{42}$). As discussed for D1 and D2, also this dark excitation can be activated when coupled to vibrational modes (see, e.g., ref 57 for the case of HBC). Higher energy excitations than P1 fall beyond the spectral range of interest (visible and near-UV bands) for coronene and HBC, while this is not the case for $C_{114}H_{30}$ and $C_{222}H_{42}$. As shown in Figure 2, higher energy peaks stem from transitions between deeper occupied and higher unoccupied MOs, carrying much weaker intensity than P1.

Proceeding now with the results for the elongated GNFs, the drastic effect on the electronic and optical properties induced by symmetry lowering from D_{6h} to D_{2h} point group is evident already from the comparison between coronene and circumbiphenyl (see Figure 4). The doubly degenerate frontier orbitals of coronene (both HOMO and LUMO) are split in circumbiphenyl (HOMO and HOMO − 1 and LUMO and LUMO + 1; Figure 4a): the existence of two inequivalent axes (x and y) in the molecular plane of the $N_L = 4$ GNF induces a different parity for HOMO and HOMO − 1, as well as for LUMO and LUMO + 1. In view of this reduced symmetry, the two lowest energy excitations (T1 and L1) are no longer dipole forbidden, as in the case of the α and p bands in the hexagonal PAHs (Figure 4b). Moreover, the main peak P1 of the D_{6h} series (Clar's β band) splits into two distinct absorption lines, L2 and T2, with 0.1 eV energy separation. These excitations are here labeled according to their polarization, as visualized in the transition density plots in Figure 5: L1 and L2 are polarized along the longitudinal (x) axis of the flake, while T1 and T2 along the transverse direction (y axis). By looking at the composition of the excitations (Table 2), one notices that T1 and T2 stem from the HOMO → LUMO + 1 and HOMO − 1 → LUMO transitions, whereas L1 and L2 are due to the HOMO → LUMO and HOMO − 1 → LUMO + 1 transitions. However, while in T1 and T2 the weight of the two transitions is almost equivalent, the dominant contribution for L1 (L2) is

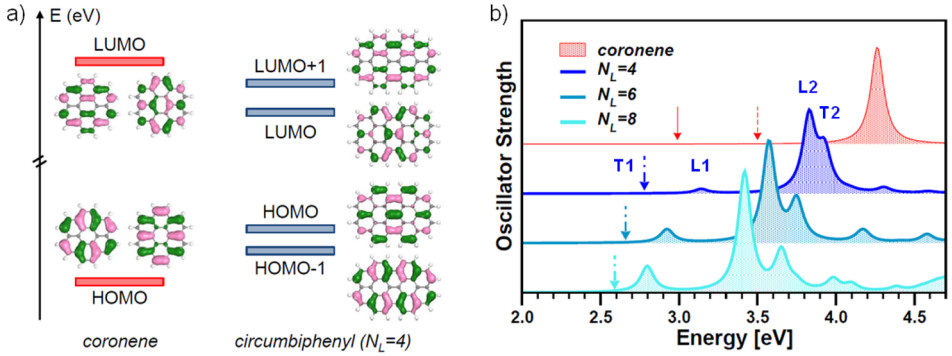

Figure 4. (a) Isosurfaces of the frontier molecular orbitals of coronene and circumbiphenyl (ribbon-like PAH with $N_L = 4$). The degeneracy of HOMO and LUMO of coronene is broken in the D_{2h} PAHs. (b) Calculated optical absorption spectra of ribbon-like PAHs, with fixed width $N_W = 7$ (about 7.4 Å) and variable length parameter ranging form $N_L = 4$ to $N_L = 8$. The main optical excitations, polarized either in the longitudinal (L, x axis) or transverse (T, y axis) direction, are indicated in the spectrum of circumbiphenyl ($N_L = 4$). The dashed−dotted arrows indicate the position of the lowest energy, weak excitation T1. For comparison, the spectrum of coronene is also shown (shaded red curve, top; see also Figure 2). The spectra are obtained through a Lorentzian broadening of 100 meV.

dx.doi.org/10.1021/jp503054j | J. Phys. Chem. A 2014, 118, 6507−6513

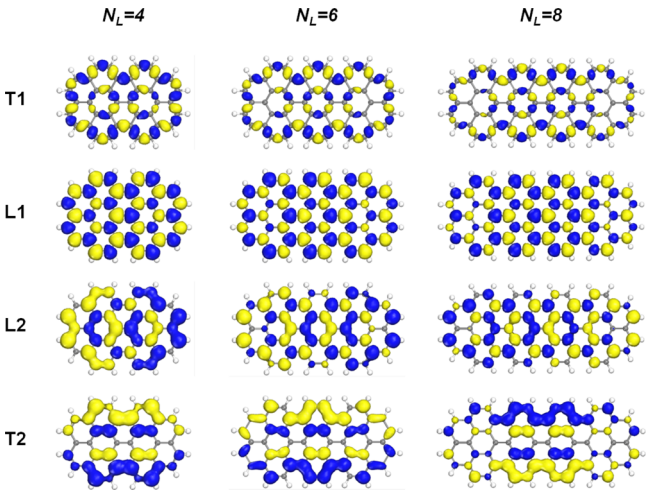

Figure 5. Transition density isosurfaces, computed as in eq 1, of the examined optical excitations of ribbon-like GNFs with D_{2h} point group symmetry.

given by HOMO → LUMO (HOMO − 1 → LUMO + 1). The anisotropy of circumbiphenyl is reflected also in the different oscillator strength of the longitudinally and transversally polarized excitations.

The relative intensity of the excitations is connected with the anisotropy, i.e., length/width ratio, of the D_{2h} PAHs. This phenomenon, which was discussed for longer flakes of the same family,[47] can be definitely clarified here for these short structures. As quantified in Table 2 and illustrated in Figure 4b, going from the N_L = 4 to the N_L = 8 ribbon-like PAHs, the oscillator strength of L1 increases by almost 1 order of magnitude, while the intensity of L2 is incremented only by a factor 1.5 (see also Table 2). A visual picture of this feature is provided by the transition densities in Figure 5, which indicates a similar modulation of L1 and L2 in the N_L = 8 PAH, compared to the stronger dipolar character of L2 for circumbiphenyl. In the case of the L1 excitation, the weight of the HOMO → LUMO increases with the length, at the expense of the HOMO − 1 → LUMO + 1 transition: in circumbiphenyl the ratio between these two single-particle transitions is about 1/3, while it decreases to less than 1/8 in the N_L = 8 PAH. The same occurs for L2, with a reversed contributions (Table 2). In the limit of very long ribbon-like PAHs with N_W = 7 and length parameter up to N_L = 20, corresponding to a length of about 88 Å, L1 and L2 present an equal oscillator strength.[47] Also here the increasing length of the flakes induces a red shift of the spectra (see Figure 4b), as observed in hexagonal PAHs (Figure 2). However, since the flake width is held fixed, the excitations with transverse polarization, T1 and T2, are very similar in all the considered D_{2h} structures: their energy is only slightly modified, and the oscillator strength is preserved along with the relative weight of the dominant MO transitions, so that on longer flakes the direct excitons will be lower than the forbidden ones.[58,59] Finally, when comparing the energy of the first active excitation for symmetric (D_{6h}) and elongated PAHs (D_{2h}), one notices that a peak at ∼2.9 eV is found for both the hexagonal $C_{114}H_{30}$ molecule and for the $C_{52}H_{20}$ flake (N_L = 6), which present a striking ratio of molecular masses with respect to each other.

CONCLUSIONS

In conclusion, we have presented a detailed quantum-chemical analysis of the effects of size and anisotropy on the optical properties of two prototypical classes of PAHs, with D_{6h} and D_{2h} symmetry. Having ruled out spurious effects with the

Table 2. Summary of the Main Optical Excitations, I, of Rectangular PAHs (D_{2h} Point Group Symmetry), Including Energy, Oscillator Strength (OS), and Composition in Terms of Molecular Orbital Transitions with the Corresponding CI Coefficients and Weight; Note That Only Contributions Larger than 10% Have Been Included

molecule	I	MO transitions (weight)	$c^I_{\alpha\beta}$	energy (eV)	OS
N_L = 4 ($C_{38}H_{16}$)	T1	H → L + 1 (0.46)	−0.676	2.78	∼10^{-4}
		H − 1 → L (0.44)	0.666		
	L1	H → L (0.71)	0.842	3.14	0.17
		H − 1 → L + 1 (0.25)	0.502		
	L2	H → L (0.26)	0.507	3.83	3.05
		H − 1 → L + 1 (0.69)	−0.834		
	T2	H → L + 1 (0.42)	0.649	3.93	1.59
		H − 1 → L (0.43)	0.660		
N_L = 6 ($C_{52}H_{20}$)	T1	H → L + 1 (0.44)	0.663	2.66	∼10^{-4}
		H − 1 → L (0.42)	−0.646		
	L1	H → L (0.78)	0.884	2.92	0.54
		H − 1 → L + 1 (0.15)	0.387		
	L2	H → L (0.16)	0.403	3.57	4.04
		H − 1 → L (0.76)	−0.873		
	T2	H → L + 1 (0.43)	0.654	3.75	1.63
		H − 1 → L (0.45)	0.671		
N_L = 8 ($C_{66}H_{24}$)	T1	H → L + 1 (0.41)	0.643	2.59	∼10^{-4}
		H − 1 → L (0.39)	0.627		
	L1	H → L (0.80)	0.895	2.80	1.04
	L2	H → L (0.10)	0.323	3.42	4.82
		H − 1 → L (0.77)	0.880		
	T2	H → L + 1 (0.41)	−0.639	3.65	1.57
		H − 1 → L (0.43)	0.658		

dx.doi.org/10.1021/jp503054j | J. Phys. Chem. A 2014, 118, 6507−6513

choice of structures with purely armchair edges, the optical properties of these systems appear strongly dependent both on the size and on the anisotropy of the molecule. Most importantly, our findings indicate that the energy of the lowest energy active peak depends more crucially on the molecular symmetry than on the molecular weight, related in this case to the number of C atoms in the structure. In GNFs with D_{2h} symmetry, optically active peaks appear in the visible band already in the spectrum of circumbiphenyl ($C_{38}H_{16}$). However, only hexagonal molecules with a few hundreds of C atoms can absorb a photon in the same spectral region. The results of this work provide significant insights into the interpretation of the experimental spectra of PAHs and consequently into the physical mechanisms driving their optical absorption. Moreover, they confirm the large tunability of this class of compounds upon size and symmetry variations, regarding the optical properties. In the field of optoelectronics these outcomes represent a valuable indication in view of designing molecular nanodevices.

Finally, the detailed investigation carried out in the present study on the size and anisotropy effects on the optical spectra of representative classes of PAHs can serve as a guide for the astronomical observation of these carbon compounds. Specifically, the symmetry analysis of the main excitations in the visible region with respect of the molecular weight is a valuable indication for determining the relative abundance of medium-size aromatic molecules and hence clarifying the composition of the ISM.

AUTHOR INFORMATION

Corresponding Author

*(C.C.) E-mail: caterina.cocchi@physik.hu-berlin.de.

Present Address

[‖](C.C.) Humboldt-Universität zu Berlin, Institut für Physik and IRIS Adlershof, Zum Grossen Windkanal 6, 12489 Berlin, Germany.

Notes

The authors declare no competing financial interest.

ACKNOWLEDGMENTS

The authors are grateful to Stefano Corni and Franco Gianturco for stimulating discussions. CINECA is acknowledged for computational support. Part of this research was supported by: the Italian Ministry of Research through the national projects PRIN-GRAF (Grant No. 20105ZZTSE), FIRB-FLASHit (Grant No. RBFR12SWOJ), and the program "Progetto Premiale 2012" - project ABNANOTECH; the Italian Ministry of Foreign Affairs through the Grant No. US14GR12. M.J.C. acknowledges support from FAPESP and CNPq (Brazil).

REFERENCES

(1) Arfsten, D. P.; Schaeffer, D. J.; Mulveny, D. C. The Effects of Near Ultraviolet Radiation on the Toxic Effects of Polycyclic Aromatic Hydrocarbons in Animals and Plants: A Review. *Ecotox. Environ. Saf.* **1996**, *33*, 1−24.

(2) Clar, E.; Schoental, R. *Polycyclic Hydrocarbons*; Academic Press: New York, 1964; Vol. 2.

(3) Wu, J.; Pisula, W.; Muellen, K. Graphenes as Potential Material for Electronics. *Chem. Rev.* **2007**, *107*, 718−747.

(4) Tielens, A. Interstellar Polycyclic Aromatic Hydrocarbon Molecules. *Annu. Rev. Astron. Astrophys.* **2008**, *46*, 289−337.

(5) Leger, A.; Puget, J. Identification of the Unidentified IR Emission Features of Interstellar Dust? *Astron. Astrophys.* **1984**, *137*, L5−L8.

(6) Allamandola, L.; Tielens, A.; Barker, J. Polycyclic Aromatic Hydrocarbons and the Unidentified Infrared Emission Bands-Auto Exhaust along the Milky Way. *Astrophys. J.* **1985**, *290*, L25−L28.

(7) Léger, A.; d'Hendecourt, L. Are Polycyclic Aromatic Hydrocarbons the Carriers of the Diffuse Interstellar Bands in the Visible? *Astron. Astrophys.* **1985**, *146*, 81−85.

(8) Van der Zwet, G.; Allamandola, L. Polycyclic Aromatic Hydrocarbons and the Diffuse Interstellar Bands. *Astron. Astrophys.* **1985**, *146*, 76−80.

(9) Salama, F.; Galazutdinov, G.; Krełowski, J.; Allamandola, L.; Musaev, F. Polycyclic Aromatic Hydrocarbons and the Diffuse Interstellar Bands: A Survey. *Astrophys. J.* **1999**, *526*, 265.

(10) Allamandola, L.; Tielens, A.; Barker, J. Interstellar Polycyclic Aromatic Hydrocarbons: The Infrared Emission Bands, the Excitation/Emission Mechanism, and the Astrophysical Implications. *Astrophys. J., Suppl. Ser.* **1989**, *71*, 733−775.

(11) Allamandola, L.; Hudgins, D.; Sandford, S. Modeling the Unidentified Infrared Emission with Combinations of Polycyclic Aromatic Hydrocarbons. *Astrophys. J. Lett.* **1999**, *511*, L115.

(12) Malloci, G.; Joblin, C.; Mulas, G. On-line Database of the Spectral Properties of Polycyclic Aromatic Hydrocarbons. *Chem. Phys.* **2007**, *332*, 353−359.

(13) Bauschlicher, C., Jr.; Boersma, C.; Ricca, A.; Mattioda, A.; Cami, J.; Peeters, E.; de Armas, F. S.; Saborido, G. P.; Hudgins, D.; Allamandola, L. The NASA Ames Polycyclic Aromatic Hydrocarbon Infrared Spectroscopic Database: The Computed Spectra. *Astrophys. J., Suppl. Ser.* **2010**, *189*, 341.

(14) Malloci, G.; Mulas, G.; Joblin, C. Electronic Absorption Spectra of PAHs up to Vacuum UV. *Astron. Astrophys.* **2004**, *426*, 105−117.

(15) Rieger, R.; Müllen, K. Forever Young: Polycyclic Aromatic Hydrocarbons As Model Cases for Structural and Optical Studies. *J. Phys. Org. Chem.* **2010**, *23*, 315−325.

(16) Crawford, M.; Tielens, A.; Allamandola, L. Ionized Polycyclic Aromatic Hydrocarbons and the Diffuse Interstellar Bands. *Astrophys. J.* **1985**, *293*, L45−L48.

(17) Canuto, S.; Zerner, M. C.; Diercksen, G. H. Theoretical Studies of the Absorption Spectra of Polycyclic Aromatic Hydrocarbons. *Astrophys. J.* **1991**, *377*, 150−157.

(18) Rastogi, S.; Pathak, A.; Maurya, A. Polycyclic Aromatic Hydrocarbon Molecules in Astrophysics. *AIP Conf. Proc.* **2013**, *1543*, 49.

(19) Carelli, F.; Grassi, T.; Gianturco, F. Electron Attachment Rates for PAH Anions in the ISM and Dark Molecular Clouds: Dependence on Their Chemical Properties. *Astron. Astrophys.* **2013**, *549*, A103.

(20) Malloci, G.; Mulas, G.; Cecchi-Pestellini, C.; Joblin, C. Dehydrogenated Polycyclic Aromatic Hydrocarbons and UV Bump. *Astron. Astrophys.* **2008**, *489*, 1183−1187.

(21) Carelli, F.; Sebastianelli, F.; Baccarelli, I.; Gianturco, F. Electron-Driven Reactions in Proto-Planetary Atmospheres: Metastable Anions of Gaseous O-Benzyne. *Astrophys. J.* **2010**, *712*, 445.

(22) Carelli, F.; Sebastianelli, F.; Satta, M.; Gianturco, F. Gas-Phase Route to Polycyclic Aromatic Hydrocarbon Formation in Proto-planetary Atmospheres: Role of Stabilized Benzyne Anions. *Mon. Not. R. Astron. Soc.* **2011**, *415*, 425−430.

(23) Charles, W.; Bauschlicher, J.; Ricca, A. The Infrared Spectra of Polycyclic Aromatic Hydrocarbons with Some or All Hydrogen Atoms Removed. *Astrophys. J.* **2013**, *776*, 102.

(24) Watson, M. D.; Fechtenkötter, A.; Müllen, K. Big Is Beautiful-Aromaticity Revisited from the Viewpoint of Macromolecular and Supramolecular Benzene Chemistry. *Chem. Rev.* **2001**, *101*, 1267−1300.

(25) Doetz, F.; Brand, J. D.; Ito, S.; Gherghel, L.; Muellen, K. Synthesis of Large Polycyclic Aromatic Hydrocarbons: Variation of Size and Periphery. *J. Am. Chem. Soc.* **2000**, *122*, 7707−7717.

(26) Liu, R.; Wu, D.; Feng, X.; Müllen, K. Bottom-Up Fabrication of Photoluminescent Graphene Quantum Dots with Uniform Morphology. *J. Am. Chem. Soc.* **2011**, *133*, 15221−15223.

(27) Zhi, L.; Müllen, K. A Bottom-Up Approach from Molecular Nanographenes to Unconventional Carbon Materials. *J. Mater. Chem.* **2008**, *18*, 1472−1484.
(28) Feng, X.; Pisula, W.; Müllen, K. Large Polycyclic Aromatic Hydrocarbons: Synthesis and Discotic Organization. *Pure Appl. Chem.* **2009**, *81*, 2203−2224.
(29) Pisula, W.; Feng, X.; Muüllen, K. Charge-Carrier Transporting Graphene-Type Molecules. *Chem. Mater.* **2011**, *23*, 554−567.
(30) Grimsdale, A. C.; Müllen, K. The Chemistry of Organic Nanomaterials. *Angew. Chem., Int. Ed.* **2005**, *44*, 5592−5629.
(31) Pisula, W.; Zorn, M.; Chang, J. Y.; Müllen, K.; Zentel, R. Liquid Crystalline Ordering and Charge Transport in Semiconducting Materials. *Macromol. Rapid Commun.* **2009**, *30*, 1179−1202.
(32) AM1 and ZINDO/S calculations were performed using VAMP package included in Accelrys Materials Studio software, version 5.0 (http://accelrys.com/products/materials-studio).
(33) Wetmore, S. D.; Boyd, R. J.; Eriksson, L. A. Electron Affinities and Ionization Potentials of Nucleotide Bases. *Chem. Phys. Lett.* **2000**, *322*, 129−135.
(34) Caldas, M. J.; Pettenati, E.; Goldoni, G.; Molinari, E. Tailoring of Light Emission Properties of Functionalized Oligothiophenes. *Appl. Phys. Lett.* **2001**, *79*, 2505−2507.
(35) Dávila, L. Y. A.; Caldas, M. J. Applicability of MNDO techniques AM1 and PM3 to Ring-Structured Polymers. *J. Comput. Chem.* **2002**, *23*, 1135.
(36) Kubatkin, S.; Danilov, A.; Hjort, M.; Cornil, J.; Brédas, J.; Stuhr-Hansen, N.; Hedegård, P.; Bjørnholm, T. Single-electron transistor of a single organic molecule with access to several redox states. *Nature* **2003**, *425*, 698−701.
(37) Steglich, M.; Jäger, C.; Rouillé, G.; Huisken, F.; Mutschke, H.; Henning, T. Electronic Spectroscopy of Medium-Sized Polycyclic Aromatic Hydrocarbons: Implications for the Carriers of the 2175 Å UV Bump. *Astrophys. J. Lett.* **2010**, *712*, L16.
(38) Dewar, M. J. S.; Zoebish, E. G.; Healy, E. F.; Stewart, J. J. P. A New General Purpose Quantum Mechanical Molecular Model. *J. Am. Chem. Soc.* **1985**, *107*, 3902−3909.
(39) Ridley, J.; Zerner, M. An Intermediate Neglect of Differential Overlap Techinique for Spectroscopy: Pyrrole and the Azines. *Theor. Chem. Acta* **1973**, *32*, 111−134.
(40) Fischer-Hjalmars, I. Transition Densities of Conjugated Molecules and Intensities of Forbidden Bands. *J. Mol. Spectrosc.* **1971**, *39*, 321−331.
(41) Dreuw, A.; Head-Gordon, M. Single-Reference Ab Initio Methods for the Calculation of Excited States of Large Molecules. *Chem. Rev.* **2005**, *105*, 4009−4037.
(42) Jensen, F. *Introduction to Computational Chemistry*, 2nd ed.; Wiley: New York, 2007.
(43) Beenken, W. J.; Pullerits, T. Spectroscopic Units in Conjugated Polymers: A Quantum Chemically Founded Concept? *J. Phys. Chem. B* **2004**, *108*, 6164−6169.
(44) Krueger, B. P.; Scholes, G. D.; Fleming, G. R. Calculation of Couplings and Energy-Transfer Pathways between the Pigments of LH2 by the Ab Initio Transition Density Cube Method. *J. Phys. Chem. B* **1998**, *102*, 5378−5386.
(45) Sun, M.; Kjellberg, P.; Ma, F.; Pullerits, T. Excited State Properties of Acceptor-Substitute Carotenoids: 2D and 3D Real-Space Analysis. *Chem. Phys. Lett.* **2005**, *401*, 558−564.
(46) Stein, S. E.; Brown, R. π-Electron Properties of Large Condensed Polyaromatic Hydrocarbons. *J. Am. Chem. Soc.* **1987**, *109*, 3721−3729.
(47) Cocchi, C.; Prezzi, D.; Ruini, A.; Benassi, E.; Caldas, M. J.; Corni, S.; Molinari, E. Optical Excitations and Field Enhancement in Short Graphene Nanoribbons. *J. Phys. Chem. Lett.* **2012**, *3*, 924−929.
(48) Nakada, K.; Fujita, M.; Dresselhaus, G.; Dresselhaus, M. S. Edge State in Graphene Ribbons: Nanometer Size Effect and Edge Shape Dependence. *Phys. Rev. B* **1996**, *54*, 17954−17961.
(49) Sun, Z.; Wu, J. Open-Shell Polycyclic Aromatic Hydrocarbons. *J. Mater. Chem.* **2012**, *22*, 4151−4160.
(50) Katraro, R.; Ron, A.; Speiser, S. Photophysical Studies of Coronene and 1,12-Benzperylene. Self-Quenching, Photoquenching, Temperature Dependent Fluorescence Decay and Temperature Dependent Electronic Energy Transfer to Dye Acceptors. *Chem. Phys.* **1979**, *42*, 121−132.
(51) Weisman, J. L.; Lee, T. J.; Salama, F.; Head-Gordon, M. Time-Dependent Density Functional Theory Calculations of Large Compact Polycyclic Aromatic Hydrocarbon Cations: Implications for the Diffuse Interstellar Bands. *Astrophys. J.* **2003**, *587*, 256.
(52) Maruyama, Y.; Iwasaki, N. Absorption Spectra of Amorphous Organic Films. *Chem. Phys. Lett.* **1974**, *24*, 26−29.
(53) Orlandi, G.; Zerbetto, F. Quantum-Chemical Analysis of the Absorption and Emission Spectra of Coronene. *Chem. Phys.* **1988**, *123*, 175−185.
(54) We recently addressed this issue in the analysis of the optical spectrum of icosahedral C_{60}. A detailed discussion can be found in ref 60.
(55) An exhaustive and systematic analysis of the size effects on the electronic and optical properties of a representative set of PAHs has been recently presented by Malloci and co-workers; see ref 61.
(56) Kokkin, D. L.; Troy, T. P.; Nakajima, M.; Nauta, K.; Varberg, T. D.; Metha, G. F.; Lucas, N. T.; Schmidt, T. W. The Optical Spectrum of a Large Isolated Polycyclic Aromatic Hydrocarbon: Hexa-peri-hexabenzocoronene, $C_{42}H_{18}$. *Astrophys. J. Lett.* **2008**, *681*, L49.
(57) Rouillé, G.; Steglich, M.; Huisken, F.; Henning, T.; Müllen, K. UV/Visible Spectroscopy of Matrix-Isolated Hexa-peri-hexabenzocoronene: Interacting Electronic States and Astrophysical Context. *J. Chem. Phys.* **2009**, *131*, 204311.
(58) Prezzi, D.; Varsano, D.; Ruini, A.; Marini, A.; Molinari, E. Optical Properties of Graphene Nanoribbons: The Role of Many-Body Effects. *Phys. Rev. B* **2008**, *77*, 041404(R).
(59) Yang, L.; Cohen, M.; Louie, S. Excitonic Effects in the Optical Spectra of Graphene Nanoribbons. *Nano Lett.* **2007**, *7*, 3112−3115.
(60) Cocchi, C.; Prezzi, D.; Ruini, A.; Caldas, M. J.; Fasolino, A.; Molinari, E. Concavity Effects on the Optical Properties of Aromatic Hydrocarbons. *J. Phys. Chem. C* **2013**, *117*, 12909−12915.
(61) Malloci, G.; Cappellini, G.; Mulas, G.; Mattoni, A. Electronic and Optical Properties of Families of Polycyclic Aromatic Hydrocarbons: A Systematic (Time-Dependent) Density Functional Theory Study. *Chem. Phys.* **2011**, *384*, 19−27.